ACS APPLIED ENERGY MATERIALS

Subscriber access provided by The University of Texas at El Paso (UTEP)

Article

Single-atom and Nano-clustered Pt Catalysts for Selective CO2 Reduction

Yuan Wang, Hamidreza Arandiyan, Jason Scott, Kondo-Francois Aguey-Zinsou, and Rose Amal

ACS Appl. Energy Mater., **Just Accepted Manuscript** • DOI: 10.1021/acsaem.8b00817 • Publication Date (Web): 02 Nov 2018

ACS Publications

is published by the American Chemical Society. 1155 Sixteenth Street N.W., Washington, DC 20036

Single-atom and Nano-clustered Pt Catalysts for Selective CO_2 Reduction

Yuan Wang,[a] Hamidreza Arandiyan,[*a,b] Jason Scott,[*a] Kondo-Francois Aguey-Zinsou,[c] and Rose Amal[*a]

Miss Yuan Wang, Dr. Hamidreza Arandiyan, A/Prof. Jason Scott and Prof. Rose Amal
[a]*Particles and Catalysis Research Group, School of Chemical Engineering, The University of New South Wales, Sydney 2052, Australia*

Dr. Hamidreza Arandiyan
[b]*Laboratory of Advanced Catalysis for Sustainability, School of Chemistry, The University of Sydney, Sydney 2006, Australia*

A/Prof. Kondo-Francois Aguey-Zinsou
[c]*MERLin Group, School of Chemical Engineering, The University of New South Wales, Sydney, New South Wales 2052, Australia*

*Corresponding Authors E-mail addresses: hamid.arandiyan@sydney.edu.au (H. A.); jason.scott@unsw.edu.au (J. S.) and r.amal@unsw.edu.au (R. A.)

Abstract Increasing CO_2 emissions into the environment has triggered intensive research on CO_2 capture and utilization. Downsizing catalyst nanoparticles (NPs) to an atomic dispersion, exposing all atoms as active sites on the surface, is highly desirable to reduce noble metal usage and see improved activity on many catalytic reactions such as CO oxidation and CO_2 reduction. Yet, current studies on atomic-level understanding of the catalytic CO_2 reduction mechanism are poorly understood. Here, we report the synthesis of CeO_2 NPs decorated with atomically dispersed Pt atoms and scrutinize the reaction mechanism of CO_2 reduction catalyzed by single-atom (0.05wt%) Pt/CeO_2 and nano-clustered (2wt%) Pt/CeO_2 using *in-situ* DRIFTS. The activity results indicate that the single atom Pt/CeO_2 exhibited a 7.2 times higher reaction rate, despite a 40 times lower Pt loading than for the nano-clustered Pt/CeO_2 catalyst, and possessed good thermal stability at 500 °C. *In-situ* spectroscopy demonstrated that CO_2 activation occurs on the oxide support while H_2 dissociation occurs on the Pt metal. The single atom or nano-clustered nature of the Pt catalyst impacts on the selectivity of the reaction products towards CO or CH_4, whereby different mechanistic pathways for CO_2 reduction are suggested based on the geometric Pt arrangement. The isolated Pt atom geometry, unlike nano-clustered Pt with continuous Pt-Pt bond, weakly binds CO which restricts further hydrogenation and prevents CO poisoning. The findings illustrate the unique opportunities available for tuning catalyst activity and chemoselectivity by the rational design of atomically dispersed catalysts.

Keywords: Single atom catalyst, CO_2 reduction, nanocatalyst, Pt catalysts, in-situ spectroscopy.

Introduction

The excessive utilization of fossil fuels leads to a large amount of anthropogenic CO_2 emissions accompanied by adverse global environmental changes. Catalytic CO_2 conversion and utilization are an attractive and promising solution as they both contribute to alleviating environmental problems and have the potential to generate useful products and fuels (e.g. CO, CH_4, and CH_3OH).[1-4] Supported noble-metal catalysts, particularly Pt and Rh, have been studied for CO_2 reduction for decades due to their excellent activity and stability at low reaction temperatures.[5] However the noble metals such as Pt are expensive and of limited supply. It is commonly agreed that exposed atoms on the surface of noble metal deposits are active for catalytic oxidation-reduction reactions. It has been found that the reactivity and selectivity of the CO_2 reduction reaction is highly sensitive to the active metal nanoparticle size.[6-8] Downsizing the deposits to atomically dispersed single-atom catalysts can maximize the catalytic efficiency for various reactions while reducing cost and amount of catalyst required. Additionally, preparing a catalyst in the form of isolated single atoms can modify their catalytic behavior due to unsaturated coordination bonds and altered metal-support interaction.[9] Pt catalysts in single atom form have been found to be active for numerous reactions including oxidation, hydrogenation, and water gas shift reactions. For instance, Pt_1/Fe_2O_3 for hydrogenation,[10] Pt_1/carbon nanofibers for hydrogen production from formic acid,[11] Pt_1/TiN for the oxygen reduction reaction,[12] Pt_1/nitrogen-doped graphene for the hydrogen evolution reaction, [13] $Pt_1/m\text{-}Al_2O_3$ for selective hydrogenation and CO oxidation,[14] Pt_1/zeolite HZSM-5 for the water gas shift reaction and CO oxidation,[15] and Pt_1/Au for formic acid oxidation.[16] Very recently, Ma *et al.*[17] reported the preparation of single atom Ir_1/CeO_2 for CO_2 hydrogenation and concluded that metallic Ir was selective for methane generation while partially oxidized Ir species were selective for CO production. Yet, no evidence was provided for distinguishing the different reaction mechanisms on these two different structured catalysts. Selected studies have used electronic structure

approaches ranging from density functional theory (DFT) to correlated molecular orbital theory to examine the possible reaction mechanisms during the electrocatalytic reduction of CO_2 on isolated single atom catalysts. For example, Jung *et al.*[18] investigated the potential single atom catalysts, including Ag, Au, Co, Cu, Fe, Ir, Ni, Os, Pd, Pt, Rh and Ru, supported on defective graphene for CO_2 electroreduction. Using DFT calculations they found that Ni and Pt single atom catalysts were favorable for CH_3OH production while Os and Rh single atom catalysts were likely to produce CH_4. Computational studies by Bell *et al.* [19] showed that single atom Rh on Au (100) and Ag (100) were promising electrocatalysts for reducing CO_2 to methane. However, the DFT reaction mechanism studies indicated that the reduction occurred through completely different pathways for the two supports. A general survey of the literature reveals that direct experimental observation of the CO_2 reduction mechanism over single atom catalysts remains highly sought after. In particular, experimental evaluation of the reaction pathway and details on structure-functions for single-atom versus cluster or nanoparticle deposits is rarely reported.[20-21]

Herein, in aiming to provide clear insights into role of single atom Pt sites for CO_2 reduction, we have prepared Pt single atoms and Pt clusters anchored on CeO_2 via a simple impregnation method. *In-situ* diffuse reflectance infrared Fourier transform spectroscopy (DRIFTS), X-ray photoelectron spectroscopy (XPS) and electron paramagnetic resonance (EPR) are used to evaluate the selectivity and CO_2 reduction pathways on both Pt/CeO_2 catalysts. Based on different selectivity exhibited by the single atom and nano-clustered Pt catalysts, strategies for the rational design of selective CO_2 reduction catalysts are provided.

Results and discussion

Structural characterization

Atomically dispersed platinum (0.05wt%, namely 0.05Pt/CeO_2) and nano-clustered (2wt%, namely 2Pt/CeO_2) CeO_2-supported catalysts were synthesized using a wet-impregnation method. The preparation process and characterization details are provided in Supporting Information. The High-resolution Transmission Electron Microscopy (HRTEM) images (**Figure 1**) of the fresh samples, show that the interplanar spacing (*d* value) of the neat CeO_2 was found to be 0.320 nm (observed in the high angle annular dark field (HAADF) scanning transmission electron microscopy (STEM) in **Figure 1a**), which is in good agreement with that of the (111) crystal plane of cubic CeO_2.

The HRTEM image of 2Pt/CeO_2 shows well dispersed Pt clusters across the CeO_2 with particle sizes in the range of 0.5-3.0 nm (**Figures 1b-d**). Strong evidence of atomic Pt dispersion on the CeO_2 support for 0.05Pt/CeO_2 is provided by HAADF-STEM. **Figure S1** shows that no obvious Pt nanoparticles (NPs) or clusters are apparent on the CeO_2 surface. The images in **Figures 1e and 1f** clearly demonstrate the existence of isolated Pt atoms well dispersed on the CeO_2 (bright dots strongly contrast with cerium substrate). The line-scanning intensity profile for the highlighted area in **Figure 1f** indicates that Pt atoms are sitting on the top of the CeO_2 support. The N_2 adsorption-desorption isotherms and pore size distributions of the CeO_2 and Pt/CeO_2 catalysts are shown in **Figure S2**. Each isotherm was type II in nature with a H3-type hysteresis loop over the relative pressure range of 0.4-1, indicating the characteristic features of a mesoporous solid. As can be seen in **Table 1** the CeO_2 surface area decreased mildly following Pt loading, from 67.6 m^2/g to 50.7 m^2/g. Diffraction peaks in the XRD spectra (**Figure S3**) indicate the CeO_2 comprises a face-centered cubic fluorite structure whose crystal planes are in accordance cerianite, JCPDS PDF# 00-043-1002. No XRD signals corresponding to Pt are discernible due to the small amount and high dispersion on the CeO_2 as was shown by the HAADF-STEM images (**Figure 1**).

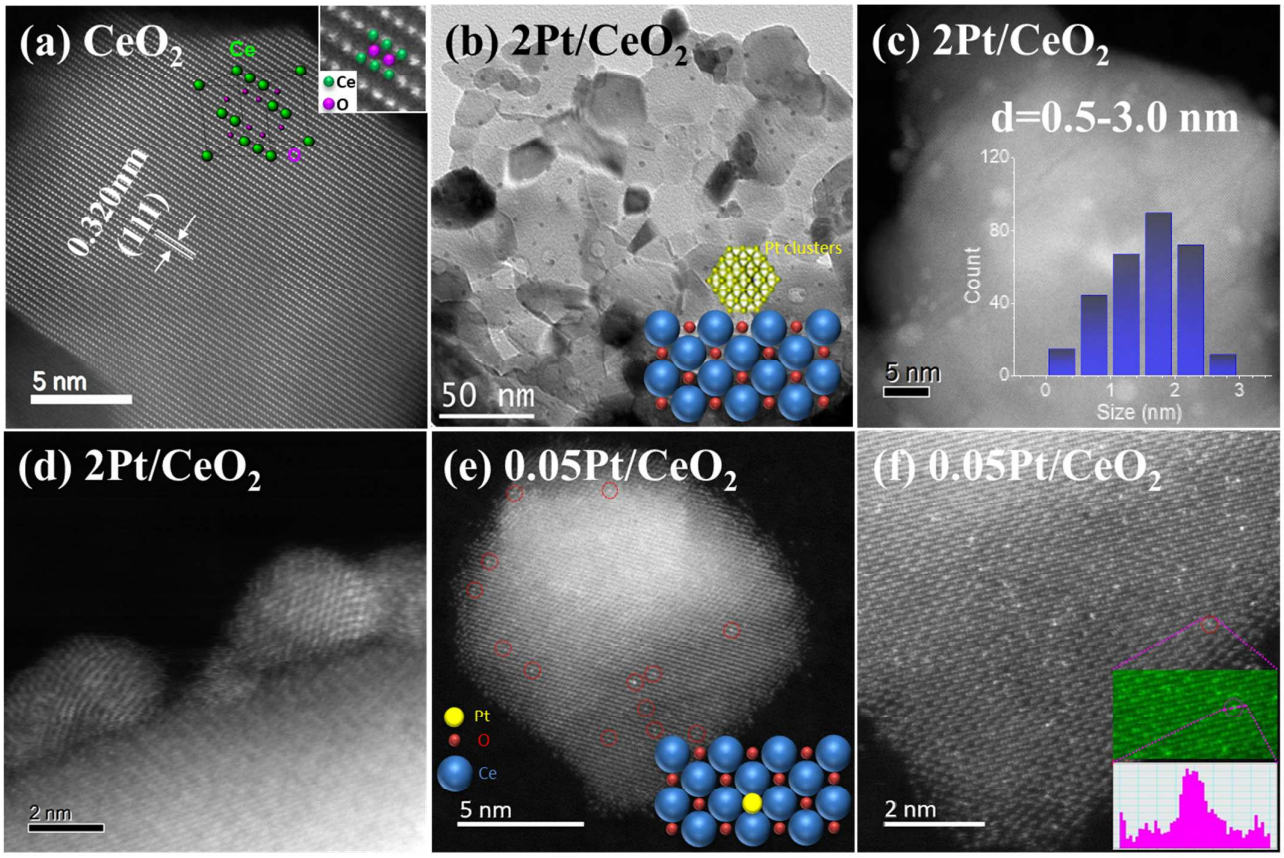

Figure 1. Structural morphology (a) HAADF-STEM image of CeO_2, (b) TEM image and (c, d) HAADF-STEM images of $2Pt/CeO_2$ (inset in (c): Pt nanoparticle size distribution for $2Pt/CeO_2$ with 300 nanoparticle counts) and (e, f) HAADF-STEM images of $0.05Pt/CeO_2$ (inset: line-scanning intensity profile obtained for the zoomed in area in (f)).

Reducibility and surface composition

The reducibility of the as-obtained CeO_2 and Pt/CeO_2 samples were studied by hydrogen temperature programmed reduction (H_2-TPR) (**Figure 2A**). The neat CeO_2 profile exhibits two reduction peaks attributable to surface Ce^{4+} reduction (455 ºC) and Ce^{4+} reduction in the bulk material (715 ºC)[22]. Upon loading Pt onto the CeO_2, both reduction peaks shifted to a lower temperature, especially the $2Pt/CeO_2$ with the lower temperature peak shifting from 455 to 187 ºC. The shift illustrates the promotional effect of Pt on the reducibility of CeO_2[22]. EPR spectroscopy was used to evaluate the surface chemistry of neat CeO_2 and Pt/CeO_2 with the spectra obtained at 50 °C shown in **Figure 2B**. The samples were pre-reduced under hydrogen at

300 °C for 1h before EPR experiments. The signals at $g_{//}$=1.953 and $g_{//}$=1.947 in 2Pt/CeO_2 and 0.05Pt/CeO_2 can be assigned to the two different Ce^{3+} sites in the bulk, stabilized by lattice defects and by easily removable ligands, respectively.[23] The Ce^{3+} ($g_{//}$=1.953) signal in neat CeO_2 was negligible however it increased upon introducing single Pt atoms and Pt nano-clusters, suggesting more surface oxygen defects are generated on the CeO_2 surface. The signal at $g_{\perp}$ =1.977 is a combination of all Ce^{3+} species located in the samples. Additionally, the strong signal at $g_{\perp}$=2.030 is attributed to the present O_2^- species bound to Ce^{4+} ions and exhibits an EPR spectrum characteristic of axial symmetry.[23] The strong O_2^- species signal in the Pt-containing materials with the difference in signal intensity between CeO_2 and Pt/CeO_2 (signal intensity increase in the order CeO_2 < 0.05Pt/CeO_2 < 2Pt/CeO_2) suggests the different ways in which O_2^- adsorbs on the surface sites. For the neat CeO_2, O_2^- is located on surface Ce^{4+} ions with both oxygen nuclei equidistant from the surface whereas the different type of Pt loadings (nano-clustered or atomically dispersed) changes the local surface environment of CeO_2 in various ways.[23] XPS was used to study the element states on the surface of the catalysts. The XPS experimental working conditions can be found in the Supporting Information. All spectra were normalized to the C1s peak = 284.8 eV for adventitious hydrocarbon.

As shown in **Figure S4**, the Ce 3d spectrum of all samples consisted of $3d_{3/2}$ and $3d_{5/2}$ pin-orbit-split doublets characteristic of CeO_2. Ce^{3+} and Ce^{4+} oxidation states can be seen in the CeO_2 and Pt-loaded CeO_2 samples, suggesting the ceria is non-stoichiometric with the present of oxygen vacancies in the ceria lattice[24]. It is noticeable that the Ce 3d profile for 0.05Pt/CeO_2 is slightly shifted towards a higher binding energy, indicating an electronic structural modification. It can be interpreted as a strong metal-support interaction between Pt atoms and the CeO_2 surface. For each sample there is an asymmetrical O1s XPS signal that can be deconvoluted into three components at binding energy (BE) values between 527-533 eV, assignable to lattice oxygen,

adsorbed oxygen and oxygen in carbonate/formate species as marked in **Figure S5**.[25-26] There is a slight increase in adsorbed oxygen species for the Pt-loaded catalysts compared to neat CeO_2.

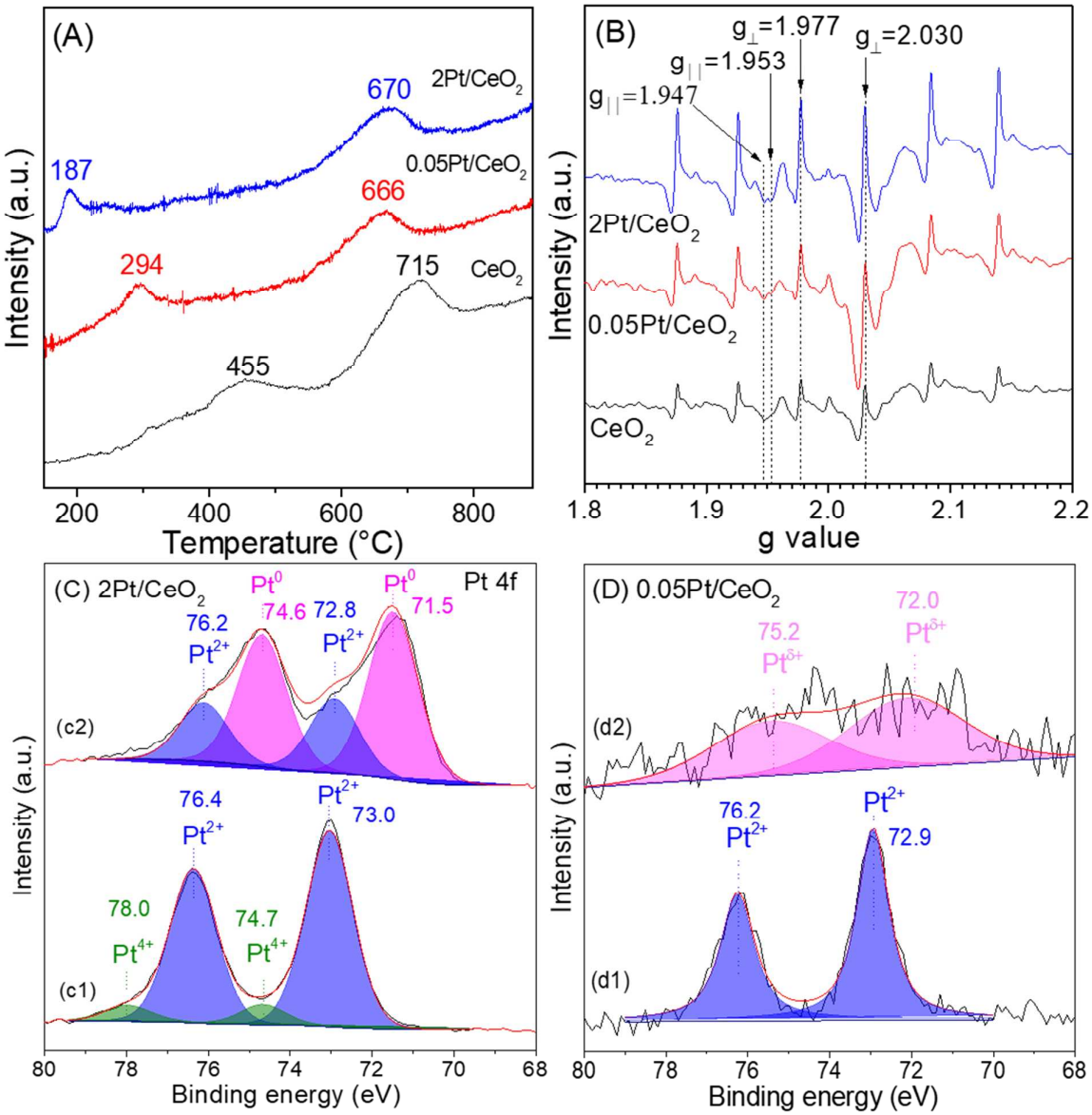

Figure 2. Reducibility and surface composition (A) H_2-TPR profiles, and (B) EPR spectra of neat CeO_2 and the Pt/CeO_2 catalysts; Pt 4f XPS spectra of (C) $2Pt/CeO_2$ and (D) $0.05Pt/CeO_2$ for (c1, d1) fresh and (c2, d2) reduced catalysts after the activity test.

Figure S6 displays the O1s XPS spectra for the Pt/CeO_2 samples following reduction at 300 °C for 1 h. The spectra can be deconvoluted into four components which represent lattice oxygen, adsorbed oxygen, hydroxyl groups and oxygen in water. Notably, the reduced $0.05Pt/CeO_2$ sample is rich in adsorbed oxygen (21.5%) and hydroxyl groups (25.7%) which is much higher

than for the reduced 2Pt/CeO_2 (9.0% and 7.04%) (**Table S1**). The XPS spectra of Pt 4f are given in **Figures 2C and 2D**. The asymmetrical Pt 4f spectrum of fresh 2Pt/CeO_2 (c1 in **Figure 2C**) can be deconvoluted into the peaks at BE = 74.7, 78.0 eV and BE = 73.0, 76.4 eV which correspond to Pt^{4+} and Pt^{2+} species, respectively, with Pt^{2+} as the major species. Fresh 0.05Pt/CeO_2 shown in d1 in **Figure 2D** has presented Pt^{2+} as the only valence state at 72.9 and 76.2 eV. CeO_2 surfaces provide a limited amount of low coordinated surface sites where Pt^{2+} ions can adsorb and remain stable during the reaction[27]. A previous DFT study [28] on Pt/CeO_2 proposed a specific structural element, a four oxygen ceria "nanopocket", which can strongly bind Pt^{2+}. Upon the reduction, the Pt^{4+} species in reduced 2Pt/CeO_2 (c2 in **Figure 2C**) disappear and the Pt^{2+} species decrease significantly with the Pt^0 peak (BE = 71.5 and 74.6 eV) emerging as the dominant species [29]. It is noted from d2 in **Figure 2D** that the binding energy of the Pt phase in 0.05Pt/CeO_2 (72.0 and 75.2 eV) after reduction is between the binding energy value of Pt^{2+} (72.8 and 76.2 eV) and Pt^0 species (71.5 and 74.6 eV), indicating an intermediate Pt state which is denoted as $Pt^{\delta+}$ ($0 < \delta < 2$). It may derive from the incomplete reduction of Pt oxide in the presence of strong metal-support interaction [30-31], implying stabilization of single atomic Pt on the ceria. Given the mismatch between a Pt atom atop the ceria lattice, non-bonding electrons will be generated on-site to form a new chemical state. The effect is similar to recent findings by our research group where DFT calculations indicated that interactions between Au with TiO_2 introduced new electronic states in the Au valence band, which then elevated the surface oxygen states to higher energies[32].

It has been reported in the literature that the strong metal-support interaction introduces new active sites which can facilitate various catalytic reactions[5]. In the single atom system, the strong metal support interaction has also been shown to stabilize the active metal atom on the support and prevent the atoms from agglomeration during high-temperature reactions[17].

Catalytic performance for CO_2 reduction

CO_2 reduction was conducted within a fixed bed reactor under a mix gas comprising CO_2 and H_2 (N_2 balance) over the temperature range 150-500 °C. Different product selectivities from the CO_2 reduction reaction were observed for the 0.05Pt/CeO_2 and 2Pt/CeO_2 catalysts (**Figure 3A**). The atomic Pt sites in 0.05Pt/CeO_2 deliver 100% CO selectivity over the entire temperature range. The Pt nano-clusters in 2Pt/CeO_2 provide 100% CO selectivity at 300 °C after which they begin to generate CH_4 from 350 °C onwards. The CH_4 selectivity continues to increase, reaching 100% at 450 °C. It is clear that the reactions requiring a large ensemble is very sensitive to the metal particle size since the various reaction intermediates and reaction steps need multi-sites to accomplish the complex assembly[30]. Comparing reverse water gas shift reaction to produce CO, the methanation reaction to form CH_4 is rather complicated assembly reaction (hydrogenation) that likely to happen on Pt nanoparticles with Pt atom bonding sties. At 450 °C 0.05Pt/CeO_2 gives almost 95% CO_2 conversion while 2Pt/CeO_2 invokes complete CO_2 conversion as illustrated in **Figure S7**. As a comparison, the activity of neat CeO_2 was assessed and showed 100% CO selectivity under all temperatures with a 50% CO_2 conversion ($T_{50\%}$) at 500 °C. It is interesting to observe that as the nano-clustered Pt decrease to an atomic level, the selectivity changes significantly. The selectivity phenomenon has been reported previously for Pt on zeolite-templated carbon for the oxygen reduction reaction whereby the isolated Pt catalyst does not follow a conventional four-electron pathway to produce H_2O, but selectively produces H_2O_2.[33] The altered selectivity of the single atom Pt catalyst here is likely a consequence of the difference in catalyst structural properties. The metal-support interaction for 0.05Pt/CeO_2 (where almost all the Pt atoms will be in direct contact with the support) can modify the electronic properties of the catalyst surface and reduced metal-metal coordination can suppress chemical reactions requiring multi-atom sites[34]. To expand on this idea, an *in-situ* DRIFTS study was conducted with the findings presented at a later point.

The CO_2 conversion rate from 175 to 250 °C (where conversion is less than 10% CO_2) was calculated on the basis of different perspectives including the exposed Pt atom number (mol_{CO2} $atom_{Pt}^{-1}$ s^{-1} as depicted in **Figure 3B**) and total mass of Pt (mol_{CO2} g_{Pt}^{-1} s^{-1} as depicted in **Figure 3C**). The calculation methods are detailed in the Supporting Information. The results show that 0.05Pt/CeO_2 exhibits a superior performance relative to 2Pt/CeO_2. For instance, at 250 °C the 0.05Pt/CeO_2 reaction rate (19.3×10^{-25} mol_{CO2} $atom_{Pt}^{-1}$ s^{-1}) is 7.6 times higher than for 2Pt/CeO_2 (2.55×10^{-25} mol_{CO2} $atom_{Pt}^{-1}$ s^{-1}) on the basis of exposed Pt atom numbers and 14 times greater than for 2Pt/CeO_2 on the basis of total Pt mass (**Figure 3B and 3C**, respectively).

The result indicates that the single atom catalyst facilitates higher catalytic conversion while using less Pt. The findings also demonstrate the unique opportunity to tune catalyst selectivity towards a desired product. To evaluate the stability of the 0.05Pt/CeO_2 catalyst, a series of recycling and duration tests were performed. The results are shown in **Figure 3D** and indicate that that there is no loss in catalyst activity over three consecutive recycles. Following the third cycle, the reaction was run continuously for 100 h at 500 °C and a gas hourly space velocity (GHSV) of ca. 48 000 mL/(g h). A small (5%) decrease in CO_2 conversion was detected over the 100 h highlighting the stability of the atomically dispersed 0.05Pt/CeO_2 catalyst. As seen in **Figure S8**, no obvious nanoparticle formation was observed for the aged 0.05Pt/CeO_2 catalyst after activity test at 500 °C.

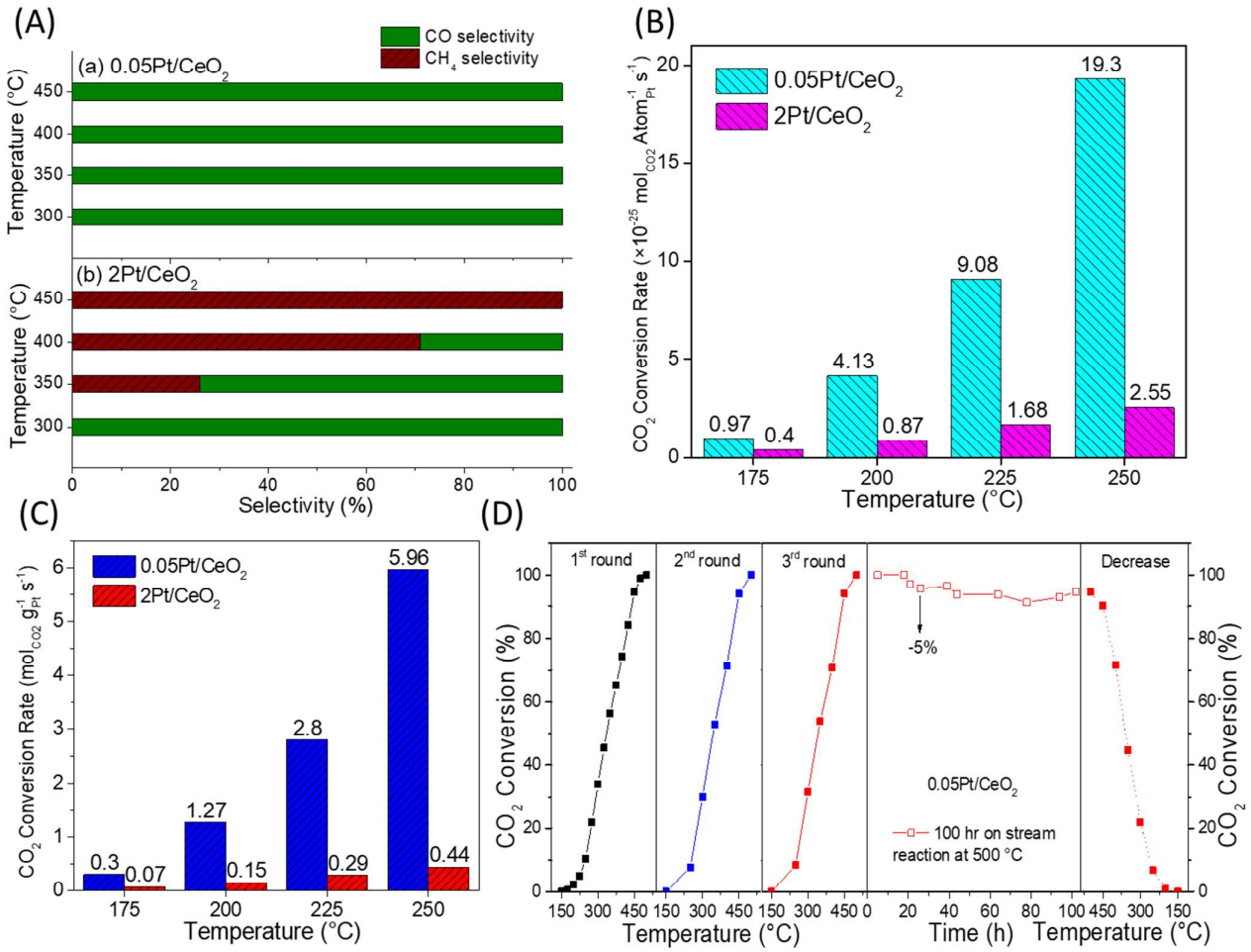

Figure 3. Catalytic performance (A) Selectivity of (a) 0.05Pt/CeO_2 and (b) 2Pt/CeO_2 toward CO and CH_4, (B) and (C) CO_2 conversion rate for 0.05Pt/CeO_2 and 2Pt/CeO_2 catalysts evaluated on the basis of exposed Pt atoms and Pt total mass, respectively, and (D) CO_2 conversion by 0.05Pt/CeO_2 over three 150 to 500 °C reaction cycles followed by reaction at 500 °C for 100 h and then cooling to 150 °C.

Identification of possible reaction pathway via in-situ DRIFTS

To provide insights into the mechanistic differences governing the selectivity of Pt supported on CeO_2 catalyst with different Pt size (atomically dispersed and nano-cluster Pt), CO_2 reduction reaction over 2Pt/CeO_2 and 0.05Pt/CeO_2 samples was further investigated by *in-situ* DRIFTS. The samples were pre-reduced at 300 °C in H_2 atmosphere (10 mL/min H_2 flow rate) for 1 h before exposure to the reactant gases ($CO_2/H_2/N_2$=2/25/70, flow rate 10 mL/min) over the temperature range 200-500 °C. In **Figure 4A, 4B** and **Figure S9**, the bands in the 3650-3600

cm^{-1} region are due to stretching vibrations of the CeO_2 surface hydroxyl groups.[35] The hydroxyl group signal for $2Pt/CeO_2$ is much weaker than for neat CeO_2 and $0.05Pt/CeO_2$ which may be due to the change of adsorption sites on CeO_2 by introducing Pt clusters. There is another deduction that the hydroxyls group on the surface of CeO_2 tends to bind on the initial Pt precursor (H_2PtCl_6) during the preparation of Pt loading catalyst by impregnation process. The observation corresponds to the earlier XPS result which showed a higher amount of surface hydroxyl species for the reduced $0.05Pt/CeO_2$ than for the $2Pt/CeO_2$ (**Figure S6**). Upon reaction gas introduction, typical signals for the gas phase CO_2 (2362 and 2332 cm^{-1}) and carbonate (1590, 1524 and 1377 cm^{-1}) are immediately identified on both Pt/CeO_2 catalysts. Among the carbonate species of Pt/CeO_2 samples, bands at 1678, 1590 and 1377 cm^{-1} can be assigned to the υ (CO_3) of bidentate carbonate[36-37], the band at 1524 cm^{-1} is due to the υ_{as} (CO_3) of monodentate carbonate[36-37], and the bands at 1456 and 1286 cm^{-1} are due to the CO and OH stretching in bicarbonate (HCO_3)[36], respectively. With an increase in temperature, the bidentate carbonate band decreases while the intensity of monodentate carbonate vibration increases. In the instance of $0.05Pt/CeO_2$ from 250 °C onward, new features in the 3000-2700 cm^{-1} region appear and these can be attributed to υ (CH) (2942 cm^{-1}) and ω (CH) (2832 and 2713 cm^{-1}) in aldehyde groups strongly bounded to $0.05Pt/CeO_2$[38]. This band intensity is gradually decreasing from 400 °C onward. The bands at 2944 and 2838 cm^{-1} for $2Pt/CeO_2$ may be due to the υ (CH) in methyne group and/or formate species[38].

Figure 4C provides the spectra over the 2250 to 1900 cm^{-1} wavenumber region so as to highlight CO adsorption which can reveal the nature of Pt in the $2Pt/CeO_2$ and $0.05Pt/CeO_2$ samples during reaction. The $0.05Pt/CeO_2$ shows only one feature peak, located at 2107 cm^{-1}, which is attributable to CO molecules linearly adsorbed on single Pt atoms. Apart from a weak band at 2107 cm^{-1}, the $2Pt/CeO_2$ exhibited a strong band at 2071 cm^{-1} which corresponds to the CO stretching on Pt NPs. Ma *et al.*[14] assigned bands at 2115 cm^{-1} and 2070-2090 cm^{-1} for

Pt/HZSM-5 zeolite to CO molecules adsorbed on single Pt atoms and NPs, respectively, which is similar to present work. In Pt/CeO_2 and Pt/Al_2O_3 systems, Jones *et al*.[39] observed a CO band on Pt^0 at 2064 cm^{-1} and a CO band on ionic Pt at 2100 cm^{-1}. Additionally, Christopher et al. [40] reported that IR stretching frequency of 2040-2090 cm^{-1} is due to the CO adsorbed to Pt_{metal} sites while the band at 2112 cm^{-1} is related to the presence of $Pt_{isolate}$ species. There is no obvious CO band on the neat CeO_2 sample, indicating that Pt provides the only adsorption sites for CO (which result is correlated to previous report[41]). The findings indicate that the Pt atoms in $0.05Pt/CeO_2$ are present in atomically dispersion, which coincides with the earlier HAADF-STEM observation.

As the temperature increases, the linear CO band on the Pt NP (2071-2043 cm^{-1}) decreases considerably and shifts to a lower wavenumber (**Figure 4A**) while the CO band representing ionic Pt (2107 cm^{-1}) in both $0.05Pt/CeO_2$ and $2Pt/CeO_2$ remains of moderate intensity. Notably, for the $0.05Pt/CeO_2$ the peak intensity of CO band is significantly lower than for $2Pt/CeO_2$ as evidenced in the IR spectra. The observations are consistent with the selectivity of $0.05Pt/CeO_2$ favoring CO as the weak CO bonding facilitates its release, directing the product toward CO. In contrast, the stronger binding of CO by the nano-clustered Pt ($2Pt/CeO_2$) leaves it more available for further reduction into methane. Alternatively, the observed low intensity of CO band in $0.05Pt/CeO_2$ could also be due to the low Pt content that limits the amount to CO adsorption. The finding also holds great promise for the utility of $0.05Pt/CeO_2$ given problems such as CO poisoning of Pt.[42] From 250 °C onward, gas phase CO is observed at 2182 cm^{-1} for both the Pt/CeO_2 catalysts while gas phase CH_4 (3013 cm^{-1}) is only present from 400 °C and above in the $2Pt/CeO_2$ sample, suggesting a temperature dynamic dependent selectivity for the Pt nano-clustered catalyst. The result correlates well with catalyst selectivity (**Figure 3A**) where the $2Pt/CeO_2$ selectively produces CH_4 from 350 °C while $0.05Pt/CeO_2$ persistently produces CO as the sole product.

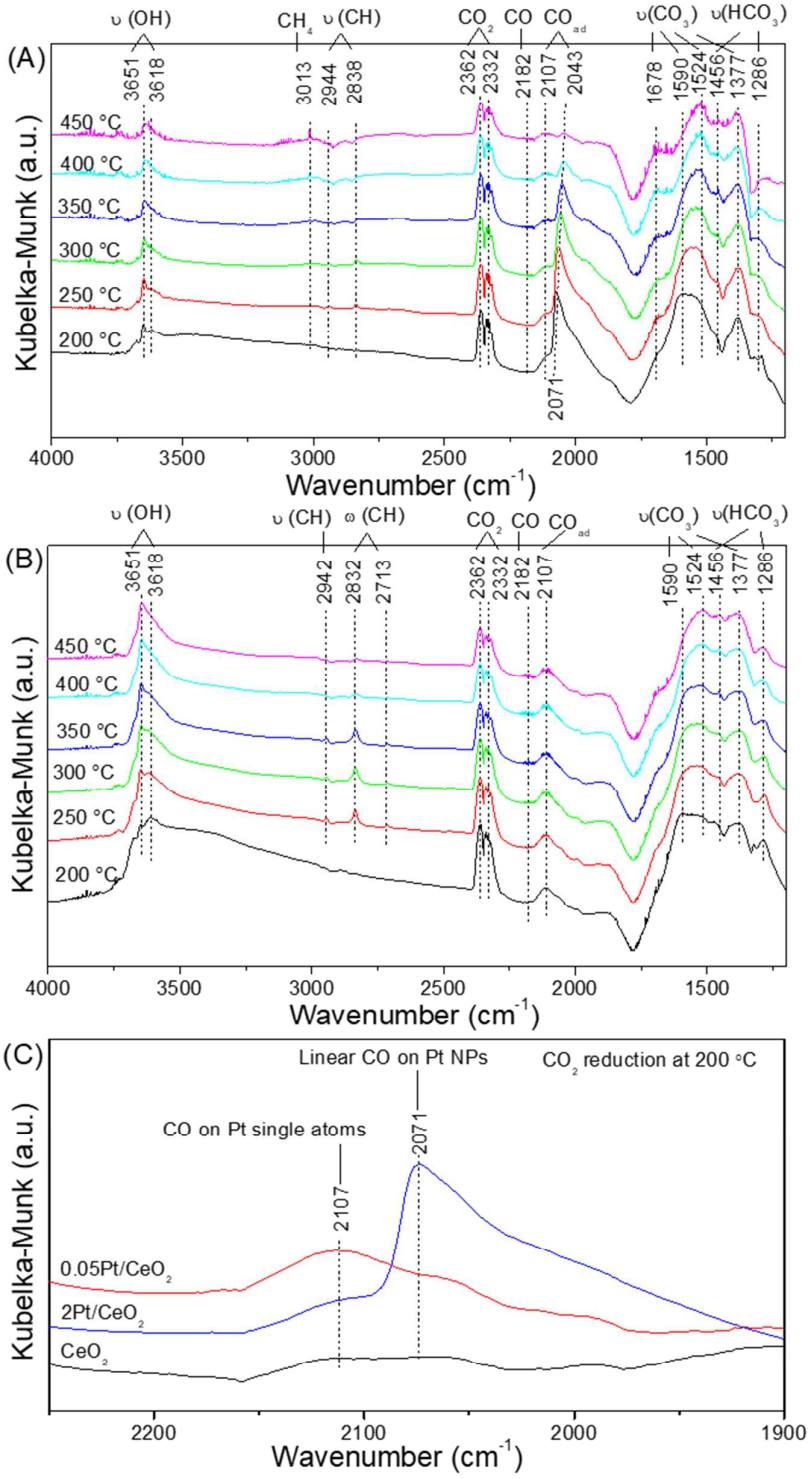

Figure 4. *In-situ* DRIFTS spectra (A) $2Pt/CeO_2$ and (B) $0.05Pt/CeO_2$ during CO_2 reduction at temperatures ranging from 200 to 450 °C, and (C) neat CeO_2 and the Pt/CeO_2 catalysts during CO_2 reduction at 220 °C (only the region between 2250 and 1900 cm^{-1} is shown to highlight CO adsorption).

Discussion of possible reaction mechanism

The findings from *in-situ* DRIFTS, XPS, EPR, and activity test in conjunction with previous reports[43-44] have been used to develop a hypothesis on the CO_2 reduction reaction mechanism at the surface of atomically dispersed Pt ($0.05Pt/CeO_2$) and nano-clustered Pt ($2Pt/CeO_2$) on CeO_2 as summarized on **Figure 5**. The *in-situ* DRIFTS spectra for $0.05Pt/CeO_2$ and $2Pt/CeO_2$ suggest they are more prone to the reverse water gas shift and CO_2 methanation reactions, respectively, which is consistent with the selectivity observed in the catalytic activity tests (**Figure 3A**). The previously reported mechanism [43] of CO_2 reduction involves the associative adsorption of CO_2 and H_2, followed by the dissociation, desorption and/or hydrogenation of the species. In this study, the rich surface oxygen defects of CeO_2 were identified from EPR analyses (signals at $g_{//}$ =1.953 and $g_{\perp}$=2.030 in **Figure 2B**), which have been described as the key sites to adsorb and active CO_2 molecules in the CO_2 reduction reaction[45]. Consequently, it is proposed that initially the CO_2 molecules attach to the surface oxygen defects (V_o) on the CeO_2 support via bonding with one of the oxygens in carbon dioxide, followed by bridging between the neighbor oxygen and CeO_2 to form a bidentate carbonate species (*in-situ* DRIFT bands at 1678, 1590, and 1377 cm^{-1}). As the temperature increases the oxygen releases from V_o to generate the monodentate species (*in-situ* DRIFT band at 1524 cm^{-1}) as shown in steps 1-3 in **Figure 5**.[46] The adatoms, H_{ad}, are thought to be provided by the dissociation of molecular H_2 on Pt.[47] According to previous theoretical studies, isolated Pt sites possess minimal activation energy for H_2 dissociation and much weaker binding of H atoms facilitating better H diffusion compared with a Pt (111) surface[48]. The dissociated H atoms can then spillover to, and react on, the CeO_2 support sites where carbonate groups are bound. The reaction occurs on the Pt/CeO_2 bifunctional catalyst where CO_2 activation happens on the oxide support and H_2 dissociation on the Pt metal, giving a reaction course similar to that detailed in mechanistic studies on Pd/Al_2O_3[43].

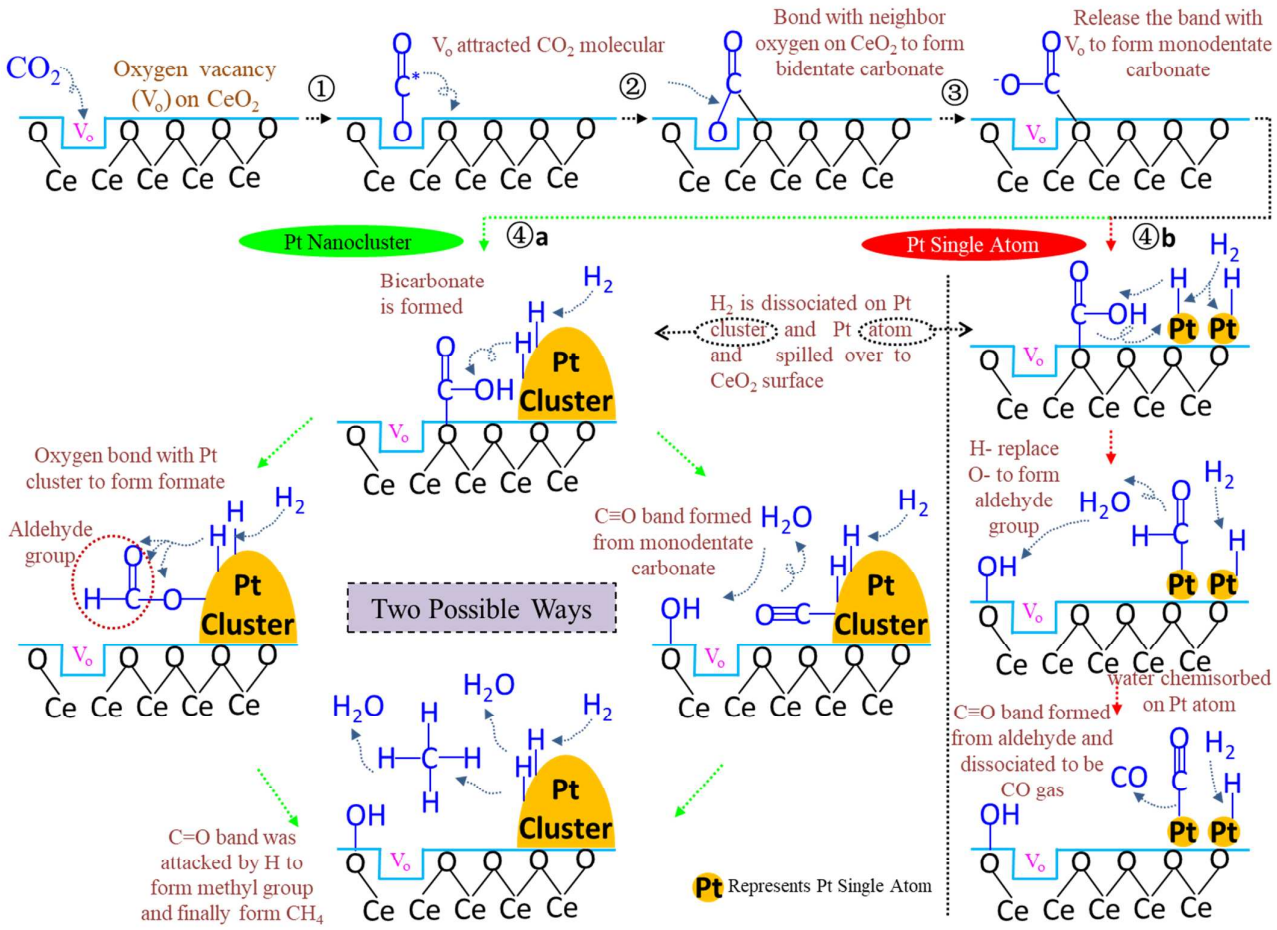

Figure 5. Proposed reaction mechanism on Pt/CeO_2. Illustration of reaction mechanism of $2Pt/CeO_2$ (pathway 4a) and $0.05Pt/CeO_2$ (pathway 4b) for CO_2 reduction.

In regards to the Pt nano-clustered catalyst ($2Pt/CeO_2$, step 4a), the bicarbonate (*in-situ* DRIFT bands at 1456 and 1286 cm^{-1}) is generated. From **Figure S9**, no bicarbonate species were observed in neat CeO_2. Therefore, the bicarbonate may be formed via the attachment of dissociated H^+ originating from the Pt. The further interaction between bicarbonate intermediate with H_{ad} on the Pt nano-clusters maybe happened in two ways: (i) generating formate (HCOO) species (*in-situ* DRIFT band at 2838 cm^{-1}) by reacting with H_{ad} dissociated from Pt clusters; and/or (ii) carbon directly bonding with the Pt cluster and the formation of a C≡O triple bond (*in-situ* DRIFT band at 2071-2043 cm^{-1}).

Table 1. BET surface areas, specific reaction rates, and XPS signal position of neat CeO_2, $0.05Pt/CeO_2$ and $2Pt/CeO_2$.

Catalyst	BET surface area $m^2\ g^{-1}$	Reaction rate at 250 ºC		Fresh sample (eV)[a]				Reduced sample (eV)[a]			
		r_a $mol_{CO2}\ g_{Pt}^{-1}\ s^{-1}$	r_a' $mol_{CO2}\ atom_{Pt}^{-1}\ s^{-1}$	Pt^{2+}		Pt^{4+}		Pt^0		Pt^{2+}	
CeO_2	67.6	-	-	-	-	-	-	-	-	-	-
$0.05Pt/CeO_2$	54.2	5.96	19.3×10^{-25}	72.9	76.2	-	-	72.0 ($Pt^{\delta+}$)		75.2 ($Pt^{\delta+}$)	
$2Pt/CeO_2$	50.7	0.44	2.55×10^{-25}	73.0	76.4	74.7	78.0	71.5	74.6	72.8	76.2

[a] Data were extracted from XPS profiles.

The proposed mechanism is based on the selectivity result which shows CO production at a lower temperature (below 300 °C) and CH_4 production at a higher temperature (above 300 °C) for $2Pt/CeO_2$, as well as the intermediate features in the IR spectra (**Figure 4A**). The two steps may occur either at the same time or are temperature dependent. H_{ad} on the Pt nano-cluster subsequently attacks C-O, C=O, and C≡O in formate and/or CO to generate CH_4 as the final product. A different reaction mechanism is proposed $0.05Pt/CeO_2$ as is shown in step 4b. The monodentate formed on CeO_2 first reacts with H_{ad} on the single Pt atom to form bicarbonate (*in-situ* DRIFT bands at 1456 and 1286 cm^{-1}). The OH^- in the bicarbonate is then replaced by H_{ad} to generate an aldehyde group (*in-situ* DRIFT bands at 2942, 2832 and 2713 cm^{-1}) followed by cleavage of C-H to form C≡O attached on a Pt single atom. As the interaction between the Pt atom and CO is weak, CO will readily desorb into the gas phase as a product. A potential reason as to why the aldehyde group is not further hydrogenated to produce CH_4 or other carbohydrates may be the strong bonding between CeO_2 and OH groups (*in-situ* DRIFT bands at 3650-3600 cm^{-1}) in the generated water which suppresses H spillover from the Pt onto the CeO_2 surface. It has been reported that CO dissociation and the CH_4 formation require a sufficient atomic hydrogen coverage on the catalyst surface[43]. Here, the OH groups may block surface sites leading to an insufficient coverage of atomic hydrogen.

Conclusions

In summary, it has been demonstrated that single atom Pt and Pt nano-clusters on a CeO_2 support exhibit distinct reaction pathway and CO_2 reduction selectivity toward CO and CH_4 formation, respectively. Additionally, the CO_2 reduction rate was found to be approximately seven times greater for the single atom Pt catalyst compared to the nano-clustered Pt catalyst when based on the number of exposed Pt atoms (mol_{CO2} $atom_{Pt}^{-1}$ s^{-1}). The isolated Pt atom arrangement invokes the weak binding of CO which restricts its further hydrogenation and minimizes CO poisoning of the catalyst surface to deliver 100% CO selectivity and excellent catalytic stability. The insights provide new opportunities to design highly active and selective single atom-based catalysts for various applications and have a great potential to reduce the costs associated with commercial noble-metal catalysts.

Methods

CeO_2 and Pt/CeO_2 preparation

The CeO_2 support was prepared by a sol-gel method using $Ce(NO_3)_3 \cdot 6H_2O$ as the precursor. The same molar amount of $Ce(NO_3)_3 \cdot 6H_2O$ and citric acid were dissolved in 20 mL water. The precursor solution was treated in an oven at 120 °C for 24 h to form a yellow gel powder which was ground and then calcined at 500 °C for 6 h in muffle furnace. The 2Pt/CeO_2 (2wt% Pt) and 0.05Pt/CeO_2 (0.05wt% Pt) were produced using a modified wetness impregnation method. 100 mg of the CeO_2 support was impregnated in 200 μL of $H_2PtCl_6 \cdot 6H_2O$ solution (with the desired amount of Pt precursor) for 3 h, before drying at 80 °C for 12 h and calcining at 450 °C for 3 h.

Catalytic activity evaluation

Catalytic performance of the catalysts for CO_2 reduction was assessed using a fixed-bed quartz tubular microreactor (i.d. = 6.0 mm) at atmospheric pressure. The catalyst sample (50 mg) was pre-treated in a gas mix of H_2 (25 mL/min) and N_2 (13 mL/min) at 300 ºC for 1 h and then in N_2

(30 mL/min) as it cooled to room temperature. The reactant gas mix containing 5 vol% CO_2, 62.5 vol% H_2 and 32.5 vol% N_2 was then introduced to the reactor at a total flow of 40 mL/min, giving a GHSV of ca. 48 000 mL/(g h). The concentrations of the reactants and products in the reactor effluent were monitored on-line by a gas chromatograph (Young Lin 6500) equipped with a TCD detector and a Carboxen-1010 PLOT column.

***In-situ* DRIFTS**

To study the reaction mechanism of CO_2 reduction in the presence of CeO_2-supported atomically dispersed Pt atoms and Pt nano-clusters, *in-situ* DRIFTS was conducted under reaction conditions. Initially, the catalyst was exposed to 10 mL/min H_2 for 1h to pre-reduce the sample. Then a 10 mL/min mix of the reaction gas comprising 2vol% CO_2, 25vol% H_2 and 73vol% N_2 was passed through the sample for 30 min to saturate the catalyst surface with the reactants. DRIFTS spectra were recorded at temperatures of 200, 250, 300, 350, 400 and 450 ^oC under the continuous reactant gas flow.

ASSOCIATED CONTENT

Supporting Information

Catalyst characterization procedures, catalytic activity measurements, HAADF-STEM, XRD patterns of neat CeO_2 and Pt/CeO_2 catalysts, N_2 adsorption-desorption isotherm and pore size distribution, XPS spectra of the samples and element spectra of neat CeO_2, 0.05Pt/CeO_2 and 2Pt/CeO_2 catalysts, activity and selectivity for CO_2 reduction over 0.05Pt/CeO_2 and 2Pt/CeO_2 TEM of aged sample. *In-situ* DRIFTS spectra of neat CeO_2 during CO_2 reduction at temperature across the range 200 to 500 °C. This is available free of charge through the Internet at http://pubs.acs.org.

AUTHOR INFORMATION

Corresponding Author Email ID:

*E-mail: hamid.arandiyan@sydney.edu.au (H. A.)

*E-mail: jason.scott@unsw.edu.au (J. S.)

*E-mail: r.amal@unsw.edu.au (R. A.)

Conflicts of interest

There are no conflicts to declare.

Acknowledgements

Y.W. thanks the University International Postgraduate Award (UIPA) program from UNSW, Sydney for the Ph.D. Scholarship. H. Arandiyan acknowledges financial support through the Vice Chancellor Research Fellowship (RG142406) program from UNSW. The authors acknowledge Drs. Rhiannon Kuchel, Katie Levick, Yin Yao, Sean Lim, and Bill Gong from the UNSW Mark Wainwright Analytical Centre and Dr. David Mitchell from the Electron Microscopy Centre, the University of Wollongong for their generous help with the SEM, TEM, HAADF-STEM and XPS analyses.

References

1. Wang, W.; Wang, S.; Ma, X.; Gong, J., Recent Advances in Catalytic Hydrogenation of Carbon Dioxide. *Chem. Soc. Rev.* **2011,** *40*, 3703-3727.
2. Wang, Y.; Arandiyan, H.; Scott, J.; Dai, H. X.; Amal, R., Hierarchically Porous Network-Like Ni/Co_3O_4: Noble Metal-Free Catalysts for Carbon Dioxide Methanation. *Adv. Sustainable Syst.* **2018,** *2*, 1700119-n/a.
3. Habibi, N.; Wang, Y.; Arandiyan, H.; Rezaei, M., Low-Temperature Synthesis of Mesoporous Nanocrystalline Magnesium Aluminate ($MgAl_2O_4$) Spinel with High Surface Area Using a Novel Modified Sol-Gel Method. *Adv. Powder Technol.* **2017,** *28*, 1249-1257.
4. Arandiyan, H.; Wang, Y.; Sun, H.; Rezaei, M.; Dai, H., Ordered Meso- and Macroporous Perovskite Oxide Catalysts for Emerging Applications. *Chem. Commun.* **2018,** *54*, 6484-6502.
5. Matsubu, J. C.; Zhang, S.; DeRita, L.; Marinkovic, N. S.; Chen, J. G.; Graham, G. W.; Pan, X.; Christopher, P., Adsorbate-Mediated Strong Metal-Support Interactions in Oxide-Supported Rh Catalysts. *Nat. Chem.* **2017,** *9*, 120-127.
6. Abdel-Mageed, A. M.; Eckle, S.; Anfang, H. G.; Behm, R. J., Selective Co Methanation in CO_2-Rich H_2 Atmospheres over a Ru/Zeolite Catalyst: The Influence of Catalyst Calcination. *J. Catal.* **2013,** *298*, 148-160.

7. Kowalczyk, Z.; Stołecki, K.; Raróg-Pilecka, W.; Miśkiewicz, E.; Wilczkowska, E.; Karpiński, Z., Supported Ruthenium Catalysts for Selective Methanation of Carbon Oxides at Very Low CO_x/H_2 Ratios. *Appl. Catal., A* **2008,** *342*, 35-39.
8. Abdel-Mageed, A. M.; Eckle, S.; Behm, R. J., High Selectivity of Supported Ru Catalysts in the Selective Co Methanation—Water Makes the Difference. *J. Am. Chem. Soc.* **2015,** *137*, 8672-8675.
9. Liu, J., Catalysis by Supported Single Metal Atoms. *ACS Catal.* **2016,** *7*, 34-59.
10. Wei, H.; Liu, X.; Wang, A.; Zhang, L.; Qiao, B.; Yang, X.; Huang, Y.; Miao, S.; Liu, J.; Zhang, T., FeO_x-Supported Platinum Single-Atom and Pseudo-Single-Atom Catalysts for Chemoselective Hydrogenation of Functionalized Nitroarenes. *Nat. Commun.* **2014,** *5*, 5634.
11. Bulushev, D. A.; Zacharska, M.; Lisitsyn, A. S.; Podyacheva, O. Y.; Hage, F. S.; Ramasse, Q. M.; Bangert, U.; Bulusheva, L. G., Single Atoms of Pt-Group Metals Stabilized by N-Doped Carbon Nanofibers for Efficient Hydrogen Production from Formic Acid. *ACS Catal.* **2016,** *6*, 3442-3451.
12. Yang, S.; Kim, J.; Tak, Y. J.; Soon, A.; Lee, H., Single-Atom Catalyst of Platinum Supported on Titanium Nitride for Selective Electrochemical Reactions. *Angew. Chem. Int. Ed.* **2016,** *55*, 2058-2062.
13. Cheng, N.; Stambula, S.; Wang, D.; Banis, M. N.; Liu, J.; Riese, A.; Xiao, B.; Li, R.; Sham, T.-K.; Liu, L.-M.; Botton, G. A.; Sun, X., Platinum Single-Atom and Cluster Catalysis of the Hydrogen Evolution Reaction. *Nat. Commun.* **2016,** *7*, 13638.
14. Zhang, Z.; Zhu, Y.; Asakura, H.; Zhang, B.; Zhang, J.; Zhou, M.; Han, Y.; Tanaka, T.; Wang, A.; Zhang, T.; Yan, N., Thermally Stable Single Atom Pt/M-Al_2O_3 for Selective Hydrogenation and CO Oxidation. *Nat. Commun.* **2017,** *8*, 16100.
15. Ding, K.; Gulec, A.; Johnson, A. M.; Schweitzer, N. M.; Stucky, G. D.; Marks, L. D.; Stair, P. C., Identification of Active Sites in CO Oxidation and Water-Gas Shift over Supported Pt Catalysts. *Science* **2015,** *350*, 189-192.
16. Yang, S.; Lee, H., Atomically Dispersed Platinum on Gold Nano-Octahedra with High Catalytic Activity on Formic Acid Oxidation. *ACS Catal.* **2013,** *3*, 437-443.
17. Li, S.; Xu, Y.; Chen, Y.; Li, W.; Lin, L.; Li, M.; Deng, Y.; Wang, X.; Ge, B.; Yang, C.; Yao, S.; Xie, J.; Li, Y.; Liu, X.; Ma, D., Tuning the Selectivity of Catalytic Carbon Dioxide Hydrogenation over Iridium/Cerium Oxide Catalysts with a Strong Metal-Support Interaction. *Angew. Chem. Int. Ed. Engl.* **2017,** *56*, 10761-10765.
18. Back, S.; Lim, J.; Kim, N.-Y.; Kim, Y.-H.; Jung, Y., Single-Atom Catalysts for CO_2 Electroreduction with Significant Activity and Selectivity Improvements. *Chemical Science* **2017**.
19. Cheng, M.-J.; Clark, E. L.; Pham, H. H.; Bell, A. T.; Head-Gordon, M., Quantum Mechanical Screening of Single-Atom Bimetallic Alloys for the Selective Reduction of CO_2 to C1 Hydrocarbons. *ACS Catal.* **2016,** *6*, 7769-7777.
20. Matsubu, J. C.; Yang, V. N.; Christopher, P., Isolated Metal Active Site Concentration and Stability Control Catalytic CO_2 Reduction Selectivity. *J. Am. Chem. Soc.* **2015,** *137*, 3076-3084.
21. Kwak, J. H.; Kovarik, L.; Szanyi, J., CO_2 Reduction on Supported Ru/Al_2O_3 Catalysts: Cluster Size Dependence of Product Selectivity. *ACS Catal.* **2013,** *3*, 2449-2455.
22. Hwang, K.-r.; Ihm, S.-k.; Park, J.-s., Enhanced CeO_2-Supported Pt Catalyst for Water–Gas Shift Reaction. *Fuel Process. Technol.* **2010,** *91*, 729-736.
23. Abi-aad, E.; Bechara, R.; Grimblot, J.; Aboukais, A., Preparation and Characterization of Ceria under an Oxidizing Atmosphere. Thermal Analysis, XPS, and EPR Study. *Chem. Mater.* **1993,** *5*, 793-797.
24. Jain, R.; Poyraz, A. S.; Gamliel, D. P.; Valla, J.; Suib, S. L.; Maric, R., Comparative Study for Low Temperature Water-Gas Shift Reaction on Pt/Ceria Catalysts: Role of Different Ceria Supports. *Appl. Catal., A* **2015,** *507*, 1-13.
25. Liang, F.; Yu, Y.; Zhou, W.; Xu, X.; Zhu, Z., Highly Defective CeO_2 as a Promoter for Efficient and Stable Water Oxidation. *J. Mater. Chem. A* **2015,** *3*, 634-640.

26. Wang, Y.; Arandiyan, H.; Tahini, H. A.; Scott, J.; Tan, X.; Dai, H.; Gale, J. D.; Rohl, A. L.; Smith, S. C.; Amal, R., The Controlled Disassembly of Mesostructured Perovskites as an Avenue to Fabricating High Performance Nanohybrid Catalysts. *Nat. Commun.* **2017,** *8*, 15553.
27. Dvořák, F.; Farnesi Camellone, M.; Tovt, A.; Tran, N.-D.; Negreiros, F. R.; Vorokhta, M.; Skála, T.; Matolínová, I.; Mysliveček, J.; Matolín, V.; Fabris, S., Creating Single-Atom Pt-Ceria Catalysts by Surface Step Decoration. *Nat. Commun.* **2016,** *7*, 10801.
28. Bruix, A.; Lykhach, Y.; Matolínová, I.; Neitzel, A.; Skála, T.; Tsud, N.; Vorokhta, M.; Stetsovych, V.; Ševčíková, K.; Mysliveček, J.; Fiala, R.; Václavů, M.; Prince, K. C.; Bruyère, S.; Potin, V.; Illas, F.; Matolín, V.; Libuda, J.; Neyman, K. M., Maximum Noble-Metal Efficiency in Catalytic Materials: Atomically Dispersed Surface Platinum. *Angew. Chem. Int. Ed.* **2014,** *53*, 10525-10530.
29. Sibin, D.; Rongming, W.; Jingyue, L., Stability Investigation of a High Number Density Pt_1/Fe_2O_3 Single-Atom Catalyst under Different Gas Environments by HAADF-STEM. *Nanotechnology* **2018,** *29*, 204002.
30. Delahay, G.; Duprez, D., Effects of Dispersion and Partial Reduction on the Catalytic Properties of Rh/Al_2O_3 Catalysts in the Steam Reforming of Mono- and Bicyclic Aromatics. *J. Catal.* **1989,** *115*, 542-550.
31. Kozlova, E. A.; Lyubina, T. P.; Nasalevich, M. A.; Vorontsov, A. V.; Miller, A. V.; Kaichev, V. V.; Parmon, V. N., Influence of the Method of Platinum Deposition on Activity and Stability of Pt/TiO_2 Photocatalysts in the Photocatalytic Oxidation of Dimethyl Methylphosphonate. *Catal. Commun.* **2011,** *12*, 597-601.
32. Wong, R. J.; Scott, J.; Low, G. K. C.; Feng, H.; Du, Y.; Hart, J. N.; Amal, R., Investigating the Effect of UV Light Pre-Treatment on the Oxygen Activation Capacity of Au/TiO_2. *Catal. Sci. Technol.* **2016,** *6*, 8188-8199.
33. Choi, C. H.; Kim, M.; Kwon, H. C.; Cho, S. J.; Yun, S.; Kim, H.-T.; Mayrhofer, K. J. J.; Kim, H.; Choi, M., Tuning Selectivity of Electrochemical Reactions by Atomically Dispersed Platinum Catalyst. *Nat. Commun.* **2016,** *7*, 10922.
34. Wang, X.; Chen, W.; Zhang, L.; Yao, T.; Liu, W.; Lin, Y.; Ju, H.; Dong, J.; Zheng, L.; Yan, W.; Zheng, X.; Li, Z.; Wang, X.; Yang, J.; He, D.; Wang, Y.; Deng, Z.; Wu, Y.; Li, Y., Uncoordinated Amine Groups of Metal–Organic Frameworks to Anchor Single Ru Sites as Chemoselective Catalysts toward the Hydrogenation of Quinoline. *J. Am. Chem. Soc.* **2017,** *139*, 9419-9422.
35. Goguet, A.; Meunier, F. C.; Tibiletti, D.; Breen, J. P.; Burch, R., Spectrokinetic Investigation of Reverse Water-Gas-Shift Reaction Intermediates over a Pt/CeO_2 Catalyst. *J. Phys. Chem. B* **2004,** *108*, 20240-20246.
36. Zhao, H.; Liu, L.; Andino, J. M.; Li, Y., Bicrystalline TiO_2 with Controllable Anatase-Brookite Phase Content for Enhanced CO_2 Photoreduction to Fuels. *J Mater Chem A Mater* **2013,** *1*, 8209-8216.
37. Das, T.; Deo, G., Synthesis, Characterization and in Situ Drifts During the CO_2 Hydrogenation Reaction over Supported Cobalt Catalysts. *J. Mol. Catal. A: Chem.* **2011,** *350*, 75-82.
38. Wang, F.; Li, C.; Zhang, X.; Wei, M.; Evans, D. G.; Duan, X., Catalytic Behavior of Supported Ru Nanoparticles on the {100}, {110}, and {111} Facet of CeO_2. *J. Catal.* **2015,** *329*, 177-186.
39. Jones, J.; Xiong, H.; DeLaRiva, A. T.; Peterson, E. J.; Pham, H.; Challa, S. R.; Qi, G.; Oh, S.; Wiebenga, M. H.; Pereira Hernández, X. I.; Wang, Y.; Datye, A. K., Thermally Stable Single-Atom Platinum-on-Ceria Catalysts Via Atom Trapping. *Science* **2016,** *353*, 150-154.
40. DeRita, L.; Dai, S.; Lopez-Zepeda, K.; Pham, N.; Graham, G. W.; Pan, X.; Christopher, P., Catalyst Architecture for Stable Single Atom Dispersion Enables Site-Specific Spectroscopic and Reactivity Measurements of CO Adsorbed to Pt Atoms, Oxidized Pt Clusters, and Metallic Pt Clusters on TiO_2. *J. Am. Chem. Soc.* **2017,** *139*, 14150-14165.
41. Kaftan, A.; Kollhoff, F.; Nguyen, T.-S.; Piccolo, L.; Laurin, M.; Libuda, J., Sensitivity of CO Oxidation toward Metal Oxidation State in Ceria-Supported Catalysts: An Operando DRIFTs-MS Study. *Catal. Sci. Technol.* **2016,** *6*, 818-828.

42. Liu, J.; Lucci, F. R.; Yang, M.; Lee, S.; Marcinkowski, M. D.; Therrien, A. J.; Williams, C. T.; Sykes, E. C. H.; Flytzani-Stephanopoulos, M., Tackling CO Poisoning with Single-Atom Alloy Catalysts. *J. Am. Chem. Soc.* **2016,** *138*, 6396-6399.
43. Wang, X.; Shi, H.; Kwak, J. H.; Szanyi, J., Mechanism of CO_2 Hydrogenation on Pd/Al_2O_3 Catalysts: Kinetics and Transient Drifts-Ms Studies. *ACS Catal.* **2015,** *5*, 6337-6349.
44. Wang, Y.; Arandiyan, H.; Scott, J.; Akia, M.; Dai, H.; Deng, J.; Aguey-Zinsou, K.-F.; Amal, R., High Performance Au–Pd Supported on 3D Hybrid Strontium-Substituted Lanthanum Manganite Perovskite Catalyst for Methane Combustion. *ACS Catal.* **2016,** *6*, 6935-6947.
45. Cheng, Z.; Sherman, B. J.; Lo, C. S., Carbon Dioxide Activation and Dissociation on Ceria (110): A Density Functional Theory Study. *J. Chem. Phys.* **2013,** *138*, 014702.
46. Sharma, S.; Sravan Kumar, K. B.; Chandnani, Y. M.; Phani Kumar, V. S.; Gangwar, B. P.; Singhal, A.; Deshpande, P. A., Mechanistic Insights into CO_2 Methanation over Ru-Substituted CeO_2. *J Phys Chem C* **2016,** *120*, 14101-14112.
47. Miao, B.; Ma, S. S. K.; Wang, X.; Su, H.; Chan, S. H., Catalysis Mechanisms of CO_2 and CO Methanation. *Catal. Sci. Technol.* **2016,** *6*, 4048-4058.
48. Lucci, F. R.; Liu, J.; Marcinkowski, M. D.; Yang, M.; Allard, L. F.; Flytzani-Stephanopoulos, M.; Sykes, E. C. H., Selective Hydrogenation of 1,3-Butadiene on Platinum–Copper Alloys at the Single-Atom Limit. *Nat. Commun.* **2015,** *6*, 8550.

Table of Contents

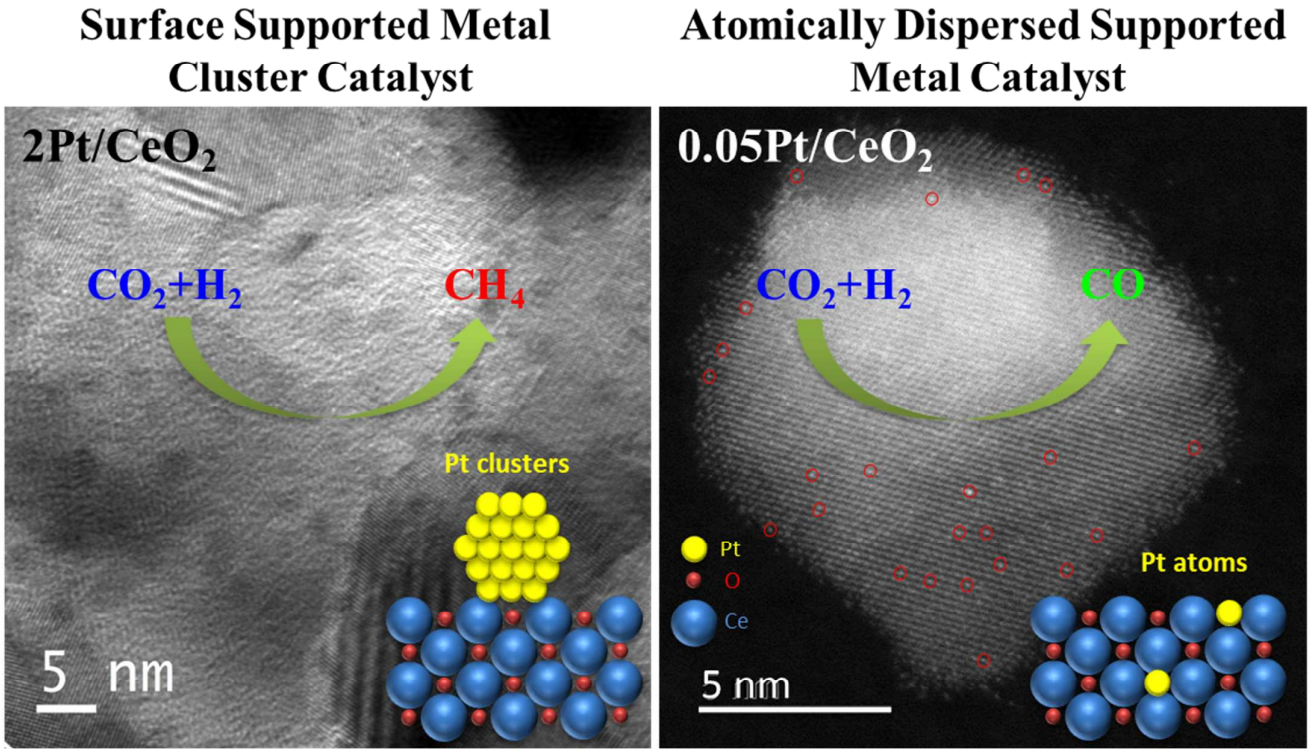

Single-atom and Nano-clustered Pt Catalysts for Selective CO_2 Reduction

Yuan Wang,[a] Hamidreza Arandiyan,[*a,b] Jason Scott,[*a] Kondo-Francois Aguey-Zinsou,[c] and Rose Amal[*a]

Keywords: Single atom catalyst, CO_2 reduction, nanocatalyst, Pt catalysts, in-situ spectroscopy.